UC Irvine
UC Irvine Previously Published Works

Title

Modeling, Simulation, and Implementation of Solar-Driven Water-Splitting Devices.

Permalink

Journal

ISSN

Authors

Xiang, Chengxiang
Weber, Adam Z
Ardo, Shane
et al.

Publication Date

DOI

Modeling, Simulation, and Implementation of Solar-Driven Water-Splitting Devices

Chengxiang Xiang*,[1] Adam Z. Weber*,[2] Shane Ardo,[3] Alan Berger,[4] YiKai Chen,[1] Robert Coridan,[5] Katherine T. Fountaine,[6] Sophia Haussener,[7] Shu Hu,[1] Rui Liu,[1], Nathan S. Lewis,[1,8], Miguel A. Modestino,[9] Matthew M. Shaner,[1,8] Meenesh R. Singh,[2] John C. Stevens,[2] Ke Sun,[1,8] Karl Walczak[2]

1. Joint Center for Artificial Photosynthesis, California Institute of Technology, Pasadena CA 91125

2. Joint Center for Artificial Photosynthesis, Lawrence Berkeley National Laboratory, Berkeley, CA 94720

3. Department of Chemistry, and Department of Chemical Engineering and Materials Science, University of California Irvine, Irvine, CA 92697

4. Air Products and Chemicals, Inc., Allentown, PA 18195

5. Department of Chemistry and Biochemistry, University of Arkansas, Fayetteville, AR

6. Nanophotonics and Plasmonics Laboratory, Northrop Grumman Aerospace Systems, Redondo Beach, CA 90278

7. Laboratory of Renewable Energy Science and Engineering, EPFL, Station 9, 1015 Lausanne, Switzerland

8. Division of Chemistry and Chemical Engineering, 210 Noyes Laboratory, 127-72, California Institute of Technology, Pasadena, CA 91125

9. School of Engineering, École Polytechnique Fédérale de Lausanne, Lausanne, 1015, Switzerland.

*To whom correspondence should be addressed: cxx@caltech.edu and azweber@lbl.gov

Dr. Chengxiang ("CX") Xiang is a Principle Investigator and Staff Scientist in Joint Center for Artificial Photosynthesis (JCAP) at California Institute of Technology. He received Ph. D in Chemical and Material Physics in University of California, Irvine in 2009. Dr. Xiang then worked with Nate Lewis as a Postdoctoral Scholar at California Institute of Technology from 2009 to 2011. Dr. Xiang research interests include design and fabrication of high efficiency solar-fuel prototypes, opto-electronic-catalytic modeling of advanced micro/nanostructured photoelectrochemical systems and multi-ion transport modeling in solution and polymer electrolytes.
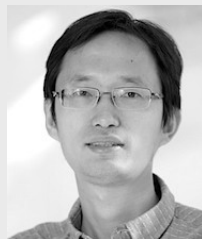
Dr. A. Z. Weber received his B.Sc and M.Sc. degrees from Tufts University in 1999, and his Ph.D. from University of California, Berkeley in 2004 under the gudiance of J. Newman. He then moved to Lawrence Berkeley National Laboratory where he is now a staff scientist, leader of the Energy Conversion Group, and thrust coordinator in at the Joint Center for Artificial Photosynthesis. His interestes and research focus on electrochemical technologies including flow batteries, fuel cells, and solar-fuel generators. He received a Presidential Early Career Award for Scientists and Engineers (PECASE) in 2012 and the Charles W. Tobias Young Investigaotr Award fo the Electrochemical Society in 2014

ABSTRACT

An integrated solar-driven water-splitting cell integrates multiple functional components and couples various photoelectrochemical (PEC) processes at different length and time scales. The overall solar-to-hydrogen (STH) conversion efficiency of such a system depends on the performance and materials properties of the individual components as well as on the component integration, overall device architecture, and system operating conditions. This review focuses on modeling- and simulation-guided development and implementation of solar-driven water-splitting prototypes from a holistic viewpoint that explores the various interplays amongst components. The underlying physics and interactions at the cell level is reviewed and discussed, followed by a review of the use of the cell model to provide target materials properties and guide the design of a range of traditional and unique device architectures.

4

I.   Introduction

To circumvent the intermittent nature of solar irradiation, one attractive approach is to store large-scale solar-converted energy in the form of chemical bonds, i.e., in an artificial photosynthetic process at an average efficiency that is significantly higher than that of most crops.[1] Significant challenges still exist for the capture, conversion, and storage of solar energy via artificial photosynthesis. Among all of the solar-driven fuel-forming devices, a solar-driven water-splitting cell has the simplest fuel-forming chemical reaction, and has demonstrated the highest efficiency, stability, and scalability.[2] Two distinctive systems, a discrete system in which a photovoltaic unit is electrically connected in series with an electrolyzer unit (PV-E) and a monolithically integrated photoelectrolysis system (PEC), have demonstrated efficient, unassisted solar-driven water-splitting on the laboratory scale. The PV-E system offers a modular approach that allows for the optimization of individual components and reduces the materials incompatibility between the power-generating and water-electrolysis units. For example, Si PV mini-modules and perovskite-based solar cells have been used recently in the PV-E design[3] and numerous demonstrations of commercial PV modules connected to electrolyzers have been performed at various scales.[4] Recent technoeconomic analyses suggest high levelized hydrogen costs in the PV-E system relative to hydrogen produced by steam reforming or grid electrolysis due to the high balance-of-system cost and the low capacity factor of the system.[5] Alternatively, the integrated PEC system leverages the simplistic design that could provide many potential advantages relative to a PV-E system and offers a unique flexibility of design for the balance of systems. [2b, 5c, 6]

5

An integrated, intrinsically safe solar-driven water-splitting device is generally comprised of light absorbers, electrocatalysts, membrane separators, and an electrolyte solution in a given system geometry. The overall solar-to-hydrogen (STH) conversion efficiency of such a system depends on the performance and materials properties of all of the individual components as well as the system design. Over the past few years, significant advances have been made in the materials discovery and development for individual components as well as in the design and implementation of solar-driven water-splitting devices at the system level. In the development of solar-driven water-splitting cells at the device level, multidimensional continuum modeling and simulation has played and continues to play a significant role in defining the target materials properties, predicting attainable device efficiencies,[7] constraining operating conditions,[8] providing cell dimensions,[9] comparing material and operating tradeoffs, and evaluating novel cell architectures and concepts.[10] Through the use of multiphysics modeling, one can understand operations and trade-offs at the device level and virtually integrate the components. Ideally, such modeling is coupled to laboratory-scale device development, which has also progressed substantially over the last few years in terms of efficiency and stability.[2b, 3, 11]

Due to the emphasize on solar-energy water splitting as a clean energy-generation technology, and the recent emergence of simulation and prototype design and material integration in this field, a review of these topics is timely. Although there have been a recent spate of reviews on the topic of solar fuels,[12] the focus of this one is unique in terms of examining the underlying multiphysics phenomena and design principles, including their implementation, from an integrated device point of view. This holistic perspective is necessary to move the field along the technology scale; throughout, comments from this point of view will

6

be made including unresolved issues. The review is structured as follows. First, the range of coupled chemical and physical phenomena that occur in a PEC system across the various lengthscales will be described from a continuum-level model basis. Namely, the light capture and transport in the semiconductor, electrocatalysis for the oxygen- and hydrogen-evolution reactions (OER and HER), ion transport in the membrane and aqueous electrolytes, product gas transport and coupled multi-component interactions between these physicochemical phenomena. Next, the simulation outputs and guidance will be explored in terms of different prototypical device systems, including unique ones, that modeling has shown to be promising.

II.   Continuum-Level Modeling

A functional solar-driven water-splitting cell integrates multiple (photo)electrochemical components that operate at different length and time scales.   Figure 1 shows a schematic illustration of various photoelectrochemical processes in an integrated solar-driven water-splitting system. Key electrochemical processes include light absorption and photoexcited charge transport in semiconductor materials, interfacial charge transport and electrocatalysis for HER and OER, multicomponent ion transport in electrolytes, and product gas transport.   At steady-state operation of the cell, these processes are fully coupled together to produce a single rate of reaction for water splitting.   As a result, it is insufficient to model individual device components in isolation or single physical phenomena in order to provide insight into the behavior of the integrated device; a coupled multiphysics, multiscale model is required.   For instance, the light absorption properties in semiconductor materials on the scale of nanometers alter the optimal morphology and structure of the photoelectrochemical assemblies at the micrometer scale, which ultimately influences the cell design and configuration at the centimeter or larger scale. This coupling is not just forward as device configurations and operation constrain the materials selection and operating points at the micrometer and nanometer scales.

A model that includes all of the critical (photo)electrochemical processes in the integrated solar-driven water-splitting device can provide important principles to guide materials discovery, evaluate novel system designs, determine the operating conditions and constraints, and allow for a predictive, quantitative understanding of the system performance.   While individual processes, such as light absorption and carrier transport in semiconductors or electrocatalysts for water-splitting reactions, have been extensively modeled and simulated, only a few efforts have

8

modeled whole system operation that couples more than two processes.[6a, 7a, 7b, 8b, 10a, 13] For example, the effects that reaction product transport has on light absorption and ionic transport are often overlooked and not quantitatively treated. In addition, the ionic transport properties across the membrane will have a strong influence on the pH conditions where an efficient, safe system can be constructed. This in turn affects the materials choices of the electrocatalysts and light absorbers that are active, stable, and compatible with such electrolytes and operating conditions. Moreover, most studies have treated the PEC systems as 0-dimensional (analytical) or 1-dimensional.[14] While this provides important trends and guidelines for solar-fuels research, the 2-dimensional or 3-dimensional effects in a real system play a critical role in understanding the operation of an actual prototype. For instance, the current density or rate of hydrogen generation distribution along the photoelectrodes has a strong dependence on the cell dimensions and thus the overall cell STH conversion efficiency.[6a, 10, 13]

Advanced multiphysics, multidimensional modeling efforts therefore are based on detailed component models but require an important additional focus on the accurate definition of the boundary conditions and exchange of information between the device components. Conservation equations (e.g. for energy, charge, momentum, and mass) and transport equations (e.g. for electromagnetic waves and species) are solved with the accurate interface conditions for the component coupling.[15] A description of an interface can simply require continuity in fluxes or can also account for complex physical phenomena (e.g. electrochemical reactions or charge transport at the semiconductor–liquid interface). This coupling introduces an additional layer of complexity because detailed component models accounting for a subset of physical phenomena might rely on the solution of another subset of equations (e.g. information of temperature

9

distribution to provide detailed temperature-dependent material properties).[16]   Consequently, coupled modeling efforts require additional external iterative solution steps, generally increasing the computational efforts and requiring special attention to ensure the model robustness and convergence.

In this section, we examine the various underlying phenomena through the lens of a coupled system model. Such analysis includes not only a discussion about how to model, including relevant physics, but also key findings in the literature. Below, we examine each component and phenomena in turn, although comments regarding the dominant interactions among them are captured within each section as per the holistic, integrated-device focus of this review.

A.   Semiconductors and light transport

The selection and optoelectronic design of the semiconductor component of a PEC water-splitting device is critical to its overall performance. The semiconductor component generates the photovoltage and photocurrent required to drive the photoelectrochemical reactions by absorbing photons with energy greater than its bandgap to generate energized electrons. Relative to the design consideration of semiconductors in a photovoltaic device, the optical and/or electronic interactions among the semiconductors, protective layers, electrocatalysts layers, solution electrolytes, and product bubbles also play a vital role in optimizing the overall PEC performance. While a comprehensive modeling and optimization that integrates all the optical and electronic effects from above has yet to be developed, significant advances have been made in determining the optimal band-gap combinations and the band energetics of the semiconductor materials for non-iterative models.[7b-d]

The selection of the optimal bandgap combinations of semiconductor materials in a solar-hydrogen device has different guiding principles than for a solid-state photovoltaic device. Under the Shockley-Queisser detailed-balance limit for photovoltaic efficiency, the photovoltage and photocurrent vary in opposing trends with the varying bandgap combinations, which results in an optimal semiconductor bandgap combination that maximizes the solar-to-electricity conversion efficiency. However, in a solar-hydrogen device, the electrochemical potential difference between HER and OER (i.e., 1.23 V under standard conditions) sets the lower bound for the required photovoltage. A photovoltage greater than 1.23 V is required to overcome the various losses in the cell including kinetics and transport as the STH conversion efficiency only depends on the product of the photocurrent and the electrochemical potential of the reaction rather than that of the photocurrent and the photovoltage, as in photovoltaics. Maximum efficiencies for water splitting are achieved with dual-junction devices that combine photovoltages from two semiconductors in series to generate the photovoltage required for water-splitting. The optimal bandgap combinations for the tandem cell structure in a solar-driven water-splitting cell have been evaluated.[7b-d, 14] For instance, as shown in Figure 2, under simulated solar illumination with an Air Mass (AM) 1.5 solar spectrum, the optimal top/bottom semiconductor band-gap combination is 1.65 eV/0.95 eV, which could yield, at the detailed-balance limit, a STH conversion efficiency of 31.1% in a system using planar Pt and RuO_x electrocatalysts and an optimized system design that minimizes the solution resistance (0.1 Ohm cm^2).[7b] The optimal bandgap combinations for the tandem photoabsorber is dependent on the performance of electrocatalysts, transport properties of membrane separators and electrolyte as well as the integrated device architecture.[7b, 7d, 17] The flexibility of the bandgap tuning in a

11

tandem cell that could trade short-circuit photocurrent for open-circuit voltage can be utilized advantageously to compensate the increase of the necessary voltage drops from various components in the system to achieve optimized device efficiency.[7a, 7b]

In terms of light management, the optical, electrical, and electrochemical interactions among semiconductors, protective coatings, and electrocatalysts in an integrated PEC system bring a whole new design space for optimized device performance relative to a discrete PV-E system, where the light management and build-in potential in the PV component is independent of the water electrolysis component. When the incident photon impinges on the surface of the PEC system, instead of absorbing by the underlying semiconductor materials, the incident light could be modulated by the components in the optical pathway between the light source and the light absorber including electrolyte, bubbles, catalysts, protective coatings, and surface structures. This modulation could attenuate the light intensity and reduce the light absorption efficiency by the light absorber through the redirection of light back to the light source in forms of reflection including diffuse/back-scattering and specular reflection (R in Figure 3a), as well as through the parasitic absorption by the various components (A in Figure 3a). In fact, such sunlight absorption by water has been found to affect adversely the performance of solar-hydrogen cells, especially those that incorporate high-efficiency multi-junction photoabsorbers. [7c]

Although the various components scatter or absorb light, this can possibly be used advantageously. When light is redirected forward by various components, this portion of light, known as deflected or forward-scattered light (S in Figure 3a), can be further absorbed by semiconductors using proper scattering. There are two types of scattering, elastic far-field

12

scattering (Figure 3a) and near-field localized surface plasmon resonance (LSPR, Figure 3b).[18] Both scattering behaviors are strongly governed by the wavelength of light, particle size/shape/morphology/density, polarization of the light, refractive index relative to surrounding media and surface structures.[19] For example, nanoparticles at the front surface have been shown to enhance the light absorption either from far-field scattering or near-field plasmonic resonance mainly on large band-gap semiconductors (E_g > 2 eV);[19b, 20] this strategy is less effective on small band-gap semiconductors (E_g < 2 eV) due to their broader spectrum utilization. More importantly, the intimate contact of semiconductors to the aqueous solution caused by sparse loading of nanoparticles often causes stability issues. Therefore, various conformal protective coatings have been developed (Figure 3c).[21] In this design, properties like solution layer thickness,[7c] electrochromism in water-oxidation catalysts, catalyst loading, refractive index/thickness of protective coatings,[21c] and surface affinity to water all strongly effect the optical absorption of semiconductors. Thus, depending on the configurations of scattering centers relative to the semiconductors, both forward and backward scattering can be utilized to enhance the light absorption of semiconductors, either at the front surface or at the back contact. Tradeoffs between catalytic activity and parasitic absorption are discussed in the next section. Moreover, gas-bubble evolution at the catalyst surface during operation could also influence the spatial and temporal absorption properties of the semiconductors located underneath. Models that account for the above mentioned optical losses and the consequent re-optimization of the bandgap combinations have yet to be developed. To date, only static models have been reported.

The loading of electrocatalysts and/or the incorporation of protective coatings not only affect the optical absorption of the semiconductors, but also the energetics in the semiconductors.

13

Beyond the absorption and scattering effects of the electrocatalysts as discussed, they also often reduce the attainable photo-voltage of the system due to increased surface recombination sites and the low barrier heights at the semiconductor/catalyst junction due to the large thermionic emission-type majority-carrier recombination. The nonuniform barrier heights from a mixture of nanoscale catalyst/semiconductor and solution/semiconductor junctions over the photoelectrode surface result in the "pinch-off" effect (Figure 3d). This has been theoretically calculated and experimentally demonstrated for Ni nanoparticles coated on n-type Si surface in a solution with a fast redox-couple.[22] However, the impact for water-splitting reactions on the attainable photo-voltage has yet to be investigated as an advanced model that accounts for the nanoscale barrier height variation and optical absorption properties of the mixed semiconductor/catalyst and semiconductor/electrolyte system has yet to be developed.

B.   Electrocatalysts

The electrochemical interfacial charge transfer between the semiconductor and the electrolyte solution (i.e., HER and OER) occurs at the electrocatalysts that are traditionally supported on the semiconductor. Two junction types, the semiconductor/electrolyte junction and the "buried" solid-state junction, are typically modeled or employed extensively experimentally. [23] The theoretical framework linking semiconductor/liquid junctions, molecular donor–acceptor systems, and heterogeneous semiconductor/metal systems has long been established.[23c, 23d] The band energetics, available states in the solution and the semiconductor and surface states can each influence the kinetic properties at the semiconductor electrodes for HER and OER. The rate of charge transfer at the surface is coupled to the rate of carrier generation and separation in the semiconductor. Surface charges are critical in a liquid-junction cell to form the depletion

14

region that affects charge transport. This characteristic comprises an important distinction from a buried-junction cell with an electrocatalyst on the surface, in which high rates of charge transfer between absorber-catalyst and catalyst-electrolyte have the potential to decouple the rate of charge transfer from the properties of the semiconductor-electrolyte junction.

The charge-transfer reactions provide the boundary conditions necessary to couple the semiconductor and electrolyte domains. Both the desired electrochemical reaction (e.g. oxidation of H_2O to O_2, H^+) and many undesired side reactions (e.g., surface recombination, crossover currents, corrosion of materials, etc.) should be considered in determining the device performance. Typically such reactions are modeled using Butler-Volmer type kinetic expressions,[15a] although microkinetic or reaction-mechanism models can be used assuming one knows the various reaction steps and intermediates. Surface roughness and changes in cross-sectional area should also be considered as they alter the geometric reaction current. Moreover, in an integrated PEC system, the catalyst performance is tied to the performance of the rest of the system (i.e., photoabsorbers, electrolytes, and membrane) due to the fact that the current is in series through them. In addition, additional layers may be included between the semiconductor and the electrocatalyst for stabilization and managing current distributions along the electrodes; they are typically modeled as conductive media using Ohm's law.

The impact of electrocatalytic properties on the STH conversion efficiency in an integrated cell has been investigated in several models.[7a, 7d, 24] For a given photoabsorber system with a certain photodiode characteristic, depending on the position of the crossing point between the photodiode curve and the water-splitting load-curve, the overall STH conversion efficiency could be extremely sensitive to the catalyst performance.[24] However, when the band-gap

15

combination of the photoabsorbers can be optimized to provide the optimal photodiode characteristic for a series of electrocatalysts with different performances, only a relatively small decrease in the optimal STH conversion efficiency is calculated (~1% improvement of the optimally attainable STH conversion efficiency for a reduction in the overpotential at 10 mA cm^{-2} by 100 mV).[7a]   Thus, the design and determination of ideal electrocatalysts cannot be uncoupled from that of photoabsorbers.

In terms of electrocatalyst placement, when electrocatalyst films are uniformly coated on the photoabsorber materials, the STH conversion efficiency of the device can be strongly affected by the parasitic absorption of the catalysts, which are either intrinsically optically opaque or electrochromic under electrolysis.[25] As a result, the optimal loading of catalysts in terms of thickness in these systems is ultrathin (<1 nm) films.[25a, 26] Developing transparent and active catalyst films, such as micro-structuring porous Pt films[27] or transparent NiO$_x$ with suppressed electrochromism under electrolysis,[21a] is required to improve cell efficiency. Alternatively, catalyst loading in a form of random or regular arrays with very low geometric filling fractions (~1 to 10%) can minimize the sensitivity of the optimal STH conversion efficiency of cells to the detailed optical properties of the catalyst material.[28]   However, the reduced catalytic area in the patterned catalyst design requires additional catalytic overpotential and/or additional transparent conductive layers, all of which may result in increased losses due to increased current flow through the electrocatalysts (i.e., higher turnover frequency). Recent studies have shown that the use of low filling fraction and low catalyst loadings provides a viable method to lower the utilization of noble metals, such as Pt, when deployed at TW scale.[28a]

C.   Electrolytes

16

The electrolyte is critical in a PEC as it enables one to complete an electrochemical circuit and the reactions to proceed. Mathematical modeling of species transport in electrolytes has different governing equations in the infinitely dilute (< 0.1 M), moderately dilute (0.1 to 1 M) and concentrated electrolytes (> 1 M).[15a, 29] In the infinitely dilute electrolyte, every species moves independently and species interact only with the solvent (water). Here, the activity of each species can be approximated by its concentration. It should be noted that the vast majority of aqueous electrolytes of interest for solar-driven water-splitting cells can be treated by either dilute or moderately dilute models. There are primarily three mechanisms of species transport: diffusion, migration, and convection where the driving forces are the concentration gradient, electric field, and velocity field, respectively. In addition to the flux equations, mass, charge, momentum, and energy conservation equations are also needed to model the system. For moderately dilute electrolytes, once must include the respective activity coefficient. For concentrated electrolytes, such as some membranes, where interactions between different species become important, advanced flux expressions that include friction coefficients and binary diffusion coefficients for multi-component electrolytes need to be employed.[15a] In addition, for a solar-hydrogen cell with spatial and temporal variations in temperature, temperature gradients can drive mass fluxes (i.e., Soret effect) and mixing in the electrolyte.

The key for modeling and choosing electrolytes is understanding the interactions and polarization losses that determine the various ion concentrations at the electrocatalysts and the subsequent device performance. These concentrations stem from transport of species (by migration and diffusion) and the resultant concentration gradients, which can be represented as a sum of ohmic and diffusion losses or concentration polarization. The ohmic loss is due to the

17

resistance of the electrolyte, and the diffusion loss originates from the species gradient in the boundary layer near each electrode due to the electrochemical reactions. Below, we discuss the issues related to losses and interactions for liquid and membrane electrolytes in turn.

C.1 Liquid electrolytes

Liquid electrolytes are ubiquitous for solar-hydrogen PECs, and contain multiple ions. Although their main responsibility is to move protons (or hydroxide ions) among the two photoelectrodes, they often contain other species that can impact the local electrocatalysts environment and hence efficiency. To model these systems, the water-dissociation/formation reaction,

$$H_2O \rightleftharpoons H^+ + OH^-$$

11* MERGEFORMAT ()

needs to be considered. In addition, various types of pH buffers, such as acetate, phosphate, borate, and carbonate, are used in solar water-splitting systems for operation at neutral or near-neutral pH values. Buffers can readily ionize or bind protons to balance pH changes in the electrolyte due to consumption/production of protons at the electrodes. The dissociation/association reaction of buffer is given as

$$HA^- \rightleftharpoons H^+ + A^{2-}$$

22* MERGEFORMAT ()

This buffer reaction is at thermal equilibrium if the rate of buffer dissociation is much faster than the rate of proton formation at the electrode. As the current density increases, the rate of proton formation can become comparable to or higher than the rate of buffer dissociation. In this case, a layer of electrolyte will form at each electrode where the concentrations of buffer species are not in equilibrium. The transport phenomena yield species concentration gradients that shift the concentrations of reacting species next to the electrode surfaces (e.g., protons, and hydroxide

18

anion) away from those present in the bulk. These pH changes at the electrodes cause an increase in the equilibrium potential of HER and OER, which impacts the electrocatalyst efficiency and associated kinetic overpotentials.

Three categories of aqueous electrolyte systems have been modeled and experimentally evaluated in recent reports on solar-driven water-splitting devices: i) strongly acidic (i.e., 1 M H_2SO_4) or strongly alkaline (i.e., 1 M KOH) solutions, ii) near-neural pH electrolytes without membrane separators, iii) near-neural pH electrolytes with membrane separators. In the strongly acidic or strongly alkaline solutions, during steady-state operation of cells at current densities that match the solar photon flux, the high conductivity of the electrolyte and near unity transference numbers of protons or hydroxide ions enable minimal electrolyte losses during steady-state operation, even with membrane separators. Modeling and simulation work have shown that with optimized system designs that include membranes to attenuate product gas crossovers as discussed in the next section, the total polarization loss in the electrolyte and membrane can be < 100 mV at an operating current density > 20 mA cm^{-2}, i.e., with STH conversion efficiencies in excess of 24%.[6a, 13]   However,   strong-acid   or   strong-base electrolytes present significant materials stability challenges for the photoabsorbers and the electrocatalysts because most of the technologically relevant photoabsorber materials, including GaAs, InP, CdTe, Si, etc, are not stable, nor are there many stable electrocatalyst materials available, in such conditions.[30]

Alternatively, significant efforts have been devoted to systems that utilize electrolytes with neutral or near-neutral pH values.[3a, 8a, 31] For near-neural pH operation without membrane

separators, STH conversion efficiency as high as 10% has been realized using a set of discrete photovoltaic cells connected in series with an electrolysis cell.[3a] Simulation has also shown that with the bubble-induced convective mixing in the cell, the polarization losses associated with the pH gradients developed at the electrode surfaces can be reduced and minimal transport loss in electrolyte can be realized for efficient solar-driven water-splitting devices.[8b] However, the lack of a membrane separator presents significant challenges for robust gas separation and collection, especially for operation at elevated temperatures and pressures with spatial and temporal variations in the system. For instance, a significant crossover of products (up to 40% H_2 in the O_2 chamber) was experimentally observed in a monolithically integrated solar-driven water-splitting device without a membrane separator.[8a]

Near-neural pH operation that incorporates a membrane separator has also been modeled and evaluated experimentally in a range of electrolytes and membrane combinations.[32] As discussed below, these membrane separators are most often ion-conduction polymers that transport nominally cations (i.e., protons) or anions (i.e., hydroxide ions), and thus are designed for use in strongly acidic or basic conditions.[8, 32] However, recent modeling and simulation work has shown that under more neutral pH conditions, such systems result in significant concentration polarization due to electrodialysis effects resulting in large pH gradients (> 6 pH units) at the surface of the electrocatalysts, even at low operating current densities (~ 1 mA cm^{-2}).[8b, 32] While sustainable photoelectrolysis has not been demonstrated at near-neural pH operation with membrane separators, certain buffer-membrane systems, e.g., imidazolium/imidazole[32] and bipolar membranes,[33] have shown promise as well as recirculation architectures.[31a]

20

C.2   Membrane separator

Membrane electrolytes are key components of PEC devices as they allow for ionic transport but block product gas crossover. Although they are typically used alongside liquid electrolytes, vapor-feed devices utilize ion-conducting membranes as the sole electrolyte,[10a, 34] see section II.D. Comprehensive review articles and textbooks have been written discussing specific material systems used as separators for water electrolysis, including proton- and anion-exchange membranes.[35]   Regardless of electrolyte pH, the material systems can be roughly categorized as microporous or ionic. Porous separators are a more mature technology, with glass and fiber-based diaphragms being used in fields such as the chlor-alkali industry. The ionic separators of interest to solar fuels are typically polymeric membranes due to the need to have high ionic conductivity near ambient temperature and to limit crossover due to pressure gradients. Various approaches to separate products without the use of a separator have been explored,[31b, 36] although these typical result in large ohmic drops.[8a]

Ion transport in the separator follows the same multicomponent diffusion equations that are used to model bulk electrolyte transport, except one may require the use of concentrated-solution theory equations.[15a] Inside the separator, the diffusion coefficients are likely to differ from their bulk values. In the case of a porous separator, corrections due to porosity and tortuosity should be considered. While porosity is a tunable parameter to some extent, both ions and gases are impacted in the same way. This presents a fundamental limitation for porous separators: a decrease in gas permeability will have a corresponding decrease in ionic conductivity. Since gas transport across the separator is undesirable, as it results typically in a parasitic loss of product and a drop in current efficiency,[37] and since small pressure gradients

21

can cause significant crossover, this requires one to utilize polymer membranes instead of microporous ones.[13, 38]

In the case of a membrane separator, interactions between the polymer and the species in solution may also have an effect, yielding different solubilities and diffusivities for ions and gases. Various transport mechanisms can occur (e.g., vehicular and hopping-like mechanisms (e.g., Grotthuss)); therefore, the density and chemical nature of the functional groups along the polymer backbone can affect ion transport,[39] and care should be taken to measure or estimate the needed transport properties accurately.[40] These transport properties may also be affected by nonideal behavior arising from morphological changes when switching liquid electrolytes or varying hydration.

Another important consideration is how to handle the interface between the separator and the bulk solution. The material balance typically ignores any interfacial mass-transfer resistance, meaning one can equate the electrochemical potential for each species across the interface as a boundary condition. For polymer membranes, this leads to a discontinuity in the potential (called the Donnan potential) due to the charged groups on the polymer, which should be accounted for.[37] Care should be taken when defining the potential to be used along with the reference states for electrochemical potentials. In most cases, the Debye length is short enough that membranes can be modeled using the electroneutrality assumption, but the Poisson and Nernst-Planck equations can be used if necessary.

Creative strategies are needed to design membranes with ideal transport properties for solar-fuel applications. Some strategies have involved modifying the annealing treatment of Nafion[TM][41] or designing block copolymers with tethered ionic-liquid functional groups.[42] It may also be possible to borrow concepts from related fields including the fuel-cell literature, where past efforts have looked at polymer-composite blends[43] and manipulation of chemical composition and chain length.[44] As mentioned above, electrodialysis effects can greatly impact device performance at near neutral pH and/or with buffers. Near neutral membranes (e.g., imidazolium/imidazole) or the use of bipolar membranes have shown some promise in reducing the electrodialysis effect by back diffusion of the neutral buffer species in the membrane. Bipolar membranes are interesting in that they allow for sustainable cell reactions at two electrolytes with different pH values.[33] While bipolar membranes have been widely used in the electrodialysis industry for producing concentrated acid and base solutions and desalinating salt water, solar-hydrogen devices that incorporate bipolar membranes have not been modeled and evaluated experimentally until very recently.[33, 45] A range of electrolyte combinations with different pH gradients exhibited sustainable solar-driven water-splitting reactions at steady state. Recent work with bipolar membranes has also shown large-area III-V tandem photoabsorbers that incorporate all earth-abundant electrocatalysts exhibited >100 hours of device stability at 10% STH conversion efficiency with a steady-state pH gradient of pH=9.3/pH=0.[46] However, the resistive loss, as well as the additional kinetic overpotential associated with water dissociation at the cation/anion internal membrane interface in the bipolar membrane constituted more than 400 mV voltage loss in the system.[46] Future work that involves improving the ohmic resistive loss in the bipolar membrane system as well as investigations of weak-acid membrane

23

systems and novel membrane structures and chemistries could potentially offer more efficient and stable operation of solar-hydrogen cells.

III.   Cell Design and Implementation

The performance of integrated solar-driven water-splitting devices is not only dependent on the properties and performances of the individual components, as discussed in the previous sections, but it also critically depends on component integration, overall device architecture, and the system operating conditions. Regardless of the various device configurations and operational conditions, the performance metrics of integrated solar-hydrogen devices can be summarized using the STH conversion efficiency and device stability, scalability, and safety. The true STH conversion efficiency of a full device should be based on the total amount of H_2 and O_2 produced and collected as a function of the incoming irradiance. In practice however, this is typically calculated from the photocurrent density under illumination, attained when the anode and cathode are shorted together assuming 100% faradaic yield for generation and collection of H_2 and O_2. The former is more rigorous and accurate, especially for fully integrated, wireless devices, and is recommended. While for a practical solar-hydrogen cell, the stability of the full devices should be evaluated by measuring the rate of hydrogen production at realistic conditions that include a diurnal cycle of solar illumination and varying temperature conditions. Due to the small size of typical laboratory-scale photoactive substrates and the lack of long-term stability in fully integrated devices, the stability is often characterized by monitoring the photocurrent density as a function of time without any external bias for continuous operation under simulated solar illumination. The scalability of the device is often evaluated by the abundance and perceived cost of the chemical elements that are required to construct the cell, while the safety of the device is often evaluated by whether the device has a robust mechanism for product gas separation and collection.   In this section, a range of device architectures (see Figure 4) that

25

could potentially meet all four-performance metrics: efficiency, stability, scalability and safety will be reviewed, including non-traditional designs, with a focus on interactions at the cell level and subsequent modeling and simulation descriptions.

A.   Planar design

One class of PEC reactor architectures utilizes macroscopic planar arrays of photoelectrodes (Fig. 4a). These photoelectrodes simultaneously provide functionality for the absorption of solar irradiation, electron and hole transport, and electrochemical reactions, and are often multi-component arrangements of nano-/micro-structured (ultra)thin layers[11d, 21f, 47] composed of the active photoelectrode, buried photovoltaic cells (traditional heterojunction cells or dye-sensitized solar cells),[48] protection and passivation layers, electrocatalytic layers, and ohmic or tunnel-junction layers. The planar electrodes have to be in contact with electrolyte in order to provide the functionality needed for a working PEC cell. Additionally, a practical design requires a semipermeable membrane to assure product separation, maximum production collection efficiency and device safety, all while enabling rapid ionic conduction.[8a, 21f] Modeling has been key in establishing design requirements of the planar electrodes, electrolyte, and separator. For an optimized multi-component photoelectrode, the design guidelines need to ensure optimized radiation absorption by the photoelectrode(s) and efficient ionic charge transport in the electrolytes and the membrane separators.

The majority of the planar photoelectrode-based designs can be categorized into back-to-back (Fig. 4a-i) and side-by-side (Fig. 4a-ii) designs. The back-to-back PEC design often contains photoabsorbers with dual-junction or triple-junction semiconductor materials to provide enough voltage to drive net water-splitting. While the back-to-back design could in principle

26

achieve the Shockley-Queisser efficiency limit for a tandem-junction or triple-junction cell, this design has very stringent materials requirements. The multi-junction photoabsorber materials need to have complementary band-gaps and similar lattice constants for epitaxial cell growth. As a result, the multi-junction photoabsorber component incorporated in the back-to-back design often contains conventional photovoltaic semiconductors (e.g., Si, GaAs, InP, CdTe, CIGS, etc.). Metal oxides and other nonconventional photoabsorber materials often lack a lattice-matched pairing semiconductor with a complementary band-gap and/or can accommodate a transparent tunnel junction between the semiconductors for the realization of a multi-junction cell architecture. Alternatively, the side-by-side design significantly relaxes the materials constraints by the use of two photoactive electrodes electrically connected in series. The lattice matching constraints and the need for optically transparent electrical contacts between the photocathode and photoanode are not applicable to the side-by-side design. Moreover, the difference in the catalytic overpotential for HER and OER and the current matching constraints between the photocathode and the photoanode can also be accommodated by tuning the ratio of the surface areas of the photoelectrodes. However, the attainable efficiency of the side-by-side design is limited to the theoretical efficiency of a single-junction absorber unless an efficient spectral-splitting method can be implemented in the cell architecture. In addition to the monolithic wireless device design, a variety of laboratory-scale demonstrations contained only a photoanode[11d, 47a, 49] or a photoanode,[50] wired to a dark counter electrode. Simulations of the differences between the wired and wireless back-to-back designs showed that the wired device design ensured shorter paths for ionic conduction compared to the wireless design.[51] When the dimension of the electrodes is not well designed, the wireless design can exhibit higher ohmic

27

overpotentials than the wired design owing to the order-of-magnitude larger electronic conductivity of wires compared to the ionic conductivity in electrolytes.

Multiphysics modeling has enabled computed efficiency evaluations of the two planar cell architectures. The size of the electrodes, the distance between the OER and the HER catalysts, and the detailed geometry for the membrane separator and solution channels play significant roles in minimizing the transport loss in the electrolyte and membrane for efficient solar water-splitting. Understanding that the path length for ion transport and the electrolyte conductivity can be limiting makes apparent that a practical (large-scale) PEC device or PEC plant based on planar electrodes cannot be envisaged as an extremely large monolithic photoabsorber device, like often proposed,[5b, 52] or as suggested by the experience of scaling photovoltaic devices. Spatially resolved computational models[6a, 13] suggested that typical electrode dimension should lie in the range of millimeters to centimeters for efficient PEC device operation.

B.   Microwire and microstructured designs

The design criteria for microwire and microstructured solar water-driven water-splitting devices (Figure 4b) are identical to those for planar architectures with the difference being that the active-device unit cells are now on the size of micrometers versus centimeters. Hence, the modeling analysis and approaches remain the same. Additionally, the ultimate metric for success, stable STH conversion efficiency at low cost and safe operation, remains constant irrespective of the active component architecture. Thus, two critical questions are: what is the risk profile associated with the potential advantages of microstructured solar water splitting devices over

28

planar equivalents if everything goes perfectly; and what are the potential disadvantages given thermodynamic and engineering constraints?

Many potential benefits of microstructured architectures as compared to planar architectures for solar-fuels production have been enumerated, but no quantitative advantage, economic- and/or performance-wise, has been shown in any real system. To date, all microwire and microstructured devices that perform unassisted solar water splitting have significantly lower STH conversion efficiencies than their planar equivalents. This performance deficit is not unique to unassisted solar water-splitting devices, it is also the case for single-junction photovoltaic and PEC devices.

The potential benefits of microstructured designs compared to planar ones include lower material usage[53], lower purity material requirements[47c], minimized ionic-transport distance[13, 54], robustness against catastrophic device failure, and fundamentally different module designs that affect the balance-of-systems requirements.[55] However, challenges include the increased complexity of epitaxial growth on the nontraditional crystallographic surface terminations present, as has been used for state-of-the-art planar designs, and the increased fabrication complexity, in general.

Single-junction photovoltaic demonstrations using Si, InP, GaAs, CdS microwire arrays have champion array efficiencies of 7.9, 13.8, 7.6, and 6%, respectively.[56] Near complete above-bandgap light absorption has been achieved in indirect bandgap Si microwire arrays through introducing scattering elements into the unoccupied space within the microwire array.[53] Many, if not all, of these photovoltaic demonstrations are directly applicable to solar water-splitting devices as they could constitute one of the two or three junctions required for efficient operation,

29

though a protective coating is necessary in most cases due to the semiconductors instability under PEC operating conditions and electrolytes as noted above. Single-junction PEC applications using microstructured arrays have focused primarily on HER. For example, single junction Si-pn$^+$ devices coated with an electrocatalyst such as Pt have shown 5.8% efficiency for hydrogen evolution.[11g, 11i]

Attempts to design and fabricate tandem-junction microstructured devices have been challenging due to the complex nature of the exposed crystal facets on which a material must be grown. Two routes have been investigated: epitaxial growth of high performance compound semiconductors (GaP, GaInP);[57] and growth of defective, nano-/microcrystalline materials that may provide intrinsic stability advantages over the known higher performance materials,[11j, 55, 58] where a maximum STH conversion efficiency of 0.12% has been reported.[11j]

For microstructured devices to achieve more than just scientific interest, clear, quantitative performance and/or economic advantages over planar equivalents must be demonstrated. One under-represented research avenue is the potential for microstructured designs to affect the balance-of-systems requirements and costs. For example, all-in-one designs could be laid out like artificial grass, again obviating the panel motif of photovoltaics and planar designs. Critical analyses of these and other potential advantages are needed to assess if and what further research on microstructured devices is warranted.

C. Particulate designs

A possible subset of microstructured designs, particulate-suspension designs remove the panel motif adopted from photovoltaics and have the potential to decrease balance-of-systems costs significantly.[5c, 59] Two types of particle-based PEC systems, termed the Type 1 reactor for a

single vessel reactor (Figure 4c-i) and the Type 2 reactor for a dual-vessel reactor (Figure 4c-ii), have been proposed conceptually and demonstrated experimentally at different levels of device integration. For the Type 1 reactor, single particle systems, including $In_{1-x}Ni_xTaO_4$ [60], $(Zn_{1+x}Ge)$ (N_2O_x) solid solution[61], $(Ga_{1-x}Zn_x)(N_{1-x}O_x)$ solid solution[62], CoO [63] and C_3N_4/CDots[64] as well as tandem-particle system, including $SrTiO_3$:Rh//$BiVO_4$ [65] and Nitrogen-doped Graphene Oxide (NGO)[66] that are electrically connected with a solid-state electron mediator have been investigated. The STH conversion efficiency in the demonstrated and stable Type 1 reactor systems is often low (< 2%). This low efficiency, coupled with a lack of a robust product-separation mechanism, presents significant challenged for large-scale implementation of such a device design.

In the Type 2 reactor, two non-contacting particles for a tandem cell are employed with a separator for product gas separation and redox-mediator transport. The Type 2 reactor leverages the tandem design and could achieve a theoretical STH conversion efficiency of ~ 25% with bandgap combinations of ~ 1.7 eV/ 1.1 eV as determined through modeling.[7b] The redox mediator, such as those based on iodine,[67] iron,[68] or cobalt[69] could provide the necessary ionic transport between the two electrochemical compartments (i.e., it acts as a molecular or ionic wire). One of the major challenges for the Type 2 reactor design is the redox selectivity at the respective catalyst sites for HER and OER. For instance, photo-driven proton reduction on the HER particle has to be much more selective over reduction of the redox mediator, despite the fact that reduction of the redox mediators is often much more thermodynamically favorable. Therefore, strategies that involve selective transport of protons and H_2 through porous oxides[70] or composite shells[71] have been employed to minimize O_2 reduction at the catalyst surface.

31

Other challenges include large distances for redox mediator transport in the solution and the membrane electrolyte, pH gradients between the two reactor vessels, and uncertain dimensions for the reactor construct; there is still a need for significant modeling and simulation work as well as experimental validation to optimize these device designs.

D.   Vapor-feed design

As discussed in section I.C., ion-conducting polymers can function as solid electrolytes in a solar-fuels device, thereby bypassing the need for liquid electrolyte, and resulting in a solid-state hydrogen generator that operates with a water-vapor feed. Operation with vapor has several advantages: the elimination of light-management and catalysis limitations from the formation of bubbles at the reaction sites, the elimination of the use of corrosive liquid electrolytes in large-scale deployment, and an overall simplification of the device design and operation.[72] These advantages come at the expense of an operation under dilute water feeds which reduces the flux of water molecules to the (photo)catalytic centers and ultimately can limit the device performance. In addition, in the absence of a liquid electrolyte, ionic transport between the cathode and anode compartment is more challenging. These requirements are similar to those encountered in catalyst layers of water-electrolysis membrane–electrode assemblies.[35b]

Water electrolysis using commercially available membrane–electrode assemblies with a water-vapor feed has demonstrated operating current densities on the order of tens of mA cm^{-2}, which is sufficient for the operation of a broad range of solar water-splitting devices.[73] Reduced current density and cell failure using vapor feed are often caused by reactant water mass-transport limitations and membrane electrolyte dehydration resulting in increased ohmic losses. A light-driven demonstration system was reported that used a membrane–electrode assembly

with photoactive TiO_2 nanoparticles incorporated into the membrane layer (Figure 4d-i). While the achieved operational current density was low in the TiO_2-based water-vapor device, the integrated absorber-in-membrane type design could lead to low-cost, high performing systems if the activity of the materials could be improved. Similar absorber-in-membrane architectures that incorporate semiconducting microwires have also been proposed, where the electrical connectivity of the device is achieved through the microwires that cross through the membrane. [55, 74]

Recent modeling studies have also provided guidelines for the design of efficient vapor-fed solar-hydrogen devices where the ionomer encapsulates the photoelectrochemical components (Figure 4d-ii). Critical device dimensions that lead to optimal water, hydrogen, and oxygen transport have been identified in various cell configurations. To achieve a current density of ~10 mA cm^{-2} in the membrane encapsulated PEC device, the ionomer film thickness needs to remain below 5 µm to avoid the formation of hydrogen or oxygen bubbles at the catalyst/membrane interface and the subsequent delamination between the membrane and the electrode.[10a] Due to the required small, thin membrane layer, a small electrode width (< 300 µm) is also necessary to maintain low ohmic resistive losses in the electrolyte. Alternatively, incorporation of a structured membrane that balances the gas and ionic transport allows the maximum electrode width to be increased to dimensions as large as a few millimeters. Furthermore, as water is consumed in the anode, anisotropies in the hydration level of the polymer electrolyte arise,[34c] which can further increase its resistance, specially as the ionomer is confined in a thin-film morphology that constrains its water uptake.[75] These dehydration effects have been recently demonstrated in a microfluidic water-vapor electrolyzer (Figure 4d-iii).[76] As

the device operated, the ohmic resistance increased due to the loss of water in the ionomer, which led to lower current densities at steady state. Overall, water-vapor feeds are promising for solar-fuels generators assuming that cost metrics and the correct current-density operating regime are amenable.

E.   Solar-concentrator-coupled PEC design

Cell designs that utilize a low-multiple concentrating solar collector (Figure 4e), such as a 10× concentrator, have great promise for large-scale, distributed solar water splitting.   A principal advantage of a sunlight-concentrating design is the potential reduction in materials, thereby resulting in a significant reduction in the system cost.[5b, 5c] Typically, these devices use a planar architecture although any of the above designs could ideally be coupled with a concentrator. However, the increased insolation could have deleterious effects on stability and efficiency, owing to such issues as increased operating temperatures and current densities. The operational photocurrent density and the open-circuit voltage of the photoabsorber materials, the catalytic performance of the electrocatalysts, and ionic transport in the electrolyte all have convolved dependences on the operational temperature and illumination intensity. For instance, while increases in the illumination intensity increase the photocurrent density and concomitantly improve the open-circuit voltage,[77] the resultant increased current density would also, however, result in an increase in the ohmic losses of the cell, as well as possibly in the reaction overpotentials.[29]

Owing to the complex interactions, there have been attempts to model and build wireless, optically concentrating solar water-splitting devices.[10b, 78] Multiphysics modeling of the steady-state operation of trough-like and axisymmetric 10x solar water-splitting devices found that, for a

design utilizing planar architecture, the absorber widths need to be reduced (to a few millimeters) in order to avoid unacceptable efficiency losses due to ohmic drop in the liquid electrolyte. Despite this, a theoretical STH conversion efficiency in excess of 29% could be achieved using tandem-junction light absorbers and state-of-the-art electrocatalysts. Beyond just steady-state operation, the daily and location-dependent variation in illumination intensity (which is compounded with the concentrating lens finite acceptance angle) and subsequent thermal rises could result in safety or lifetime issues. For example, hot days with no wind could result in temperatures above the boiling point of the electrolyte, or, at night in cold weather, the electrolyte could freeze. To analyze such real-world concerns, not only for concentrating systems but also non-concentrating ones, a robust modeling methodology that considers the concentration, PEC behavior, local weather and insolation conditions, and heat balances must be implemented; something that would benefit the field.

IV.   Summary

Modeling and simulation guided development of integrated solar-driven water-splitting devices has made significant advances in recent years.   Multidimensional multiphysics models that account for various photoelectrochemical processes have provided design guidelines for semiconductors, electrocatalysts, and both liquid and membrane electrolytes.   This review covered the guiding principles and key findings of these activities with a focus on their interactions. In addition, modeling and simulation have also revealed a range of viable device architectures that can accommodate efficient, stable, scalable, and safe solar-driven water-splitting reactions.   Although devices are being quantitatively designed and implemented, various needs still remain in terms of both capturing more complicated physics (e.g., thermal effects and bubble formation) as well as experimentally demonstrating the various tradeoffs in operation.
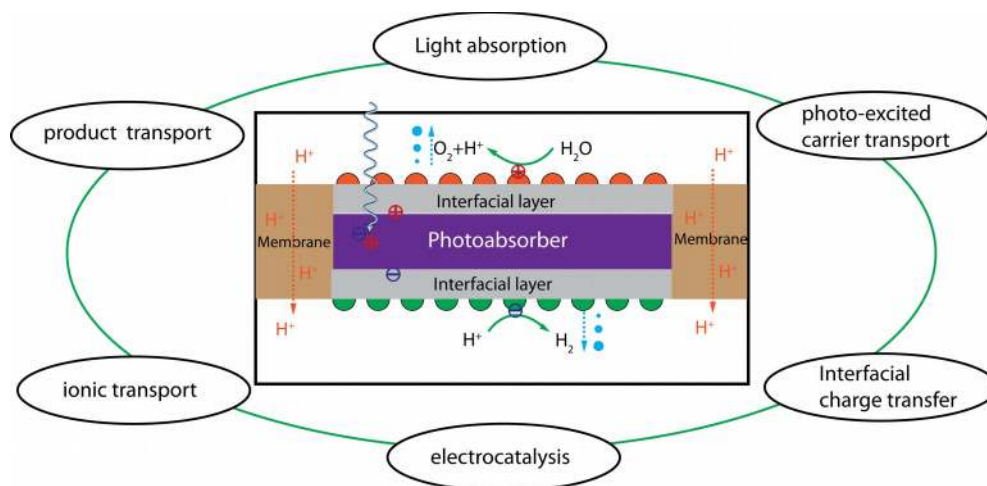
36

V. ACKNOWLEDGEMENTS

Figure 1. Schematic illustration of various coupled photoelectrochemical processes in an integrated solar-driven water-splitting cell.
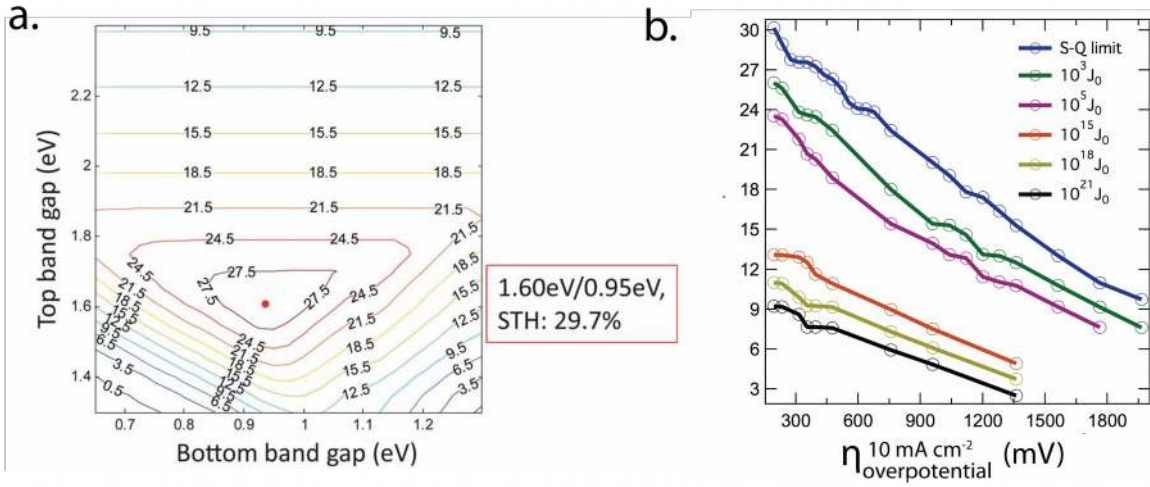
Figure 2. (a). Contour plot of water splitting efficiency for a dual junction photoelectrochemical device as a function of bottom and top semiconductor bandgap; reproduced with permission from [7b]. (b). Optimal STH conversion efficiency at all band-gap combinations as a function of the total overpotential for water-splitting at 10 mA cm^{-2}. The reverse-saturation current densities for the photoabsorbers were swept from the Shockley-Queisser (S-Q) limit, J_0, to 10^{21} J_0.
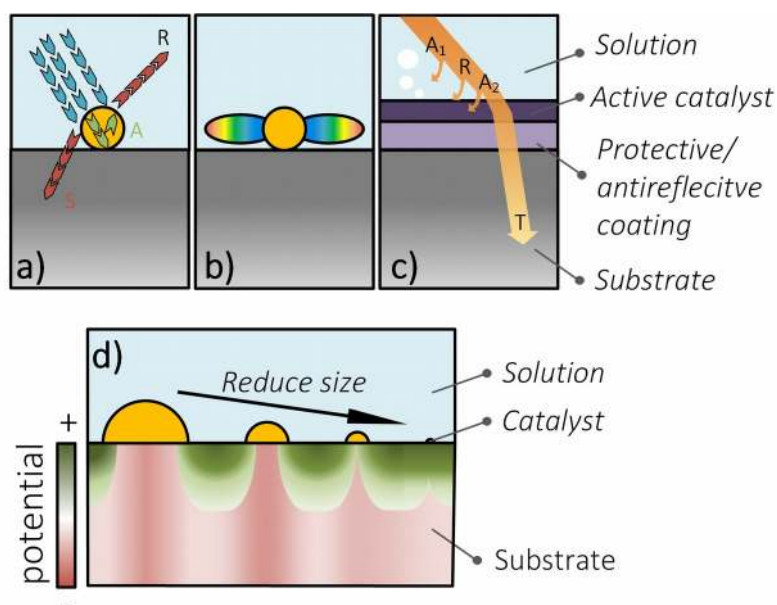
Figure 3. Schematic illustrations of optical couplings between catalysts and light absorber. a) far-field scattering for enhanced light absorption (blue arrow-incident light, red arrows-scattered and reflected light, green arrows-absorbed light, orange circle-metallic or dielectric nanoparticles), b) near-field plasmon resonance for enhanced local energy absorption , and c) optical losses in a protected photoelectrode with uniform catalyst loading (A1-absorption loss by water layer, R- reflection loss at the substrate/solution interface and scatter loss by gas bubbles, A2-absorption loss by active catalysts, and T-total optical absorption by light absorber), d) Size dependent inhomogeneous Schottky junction with solution induced inversion layer (IL), green area shows the high potential barrier at the solution semiconductor interface, red area shows the low potential barrier at the catalyst semiconductor interface.
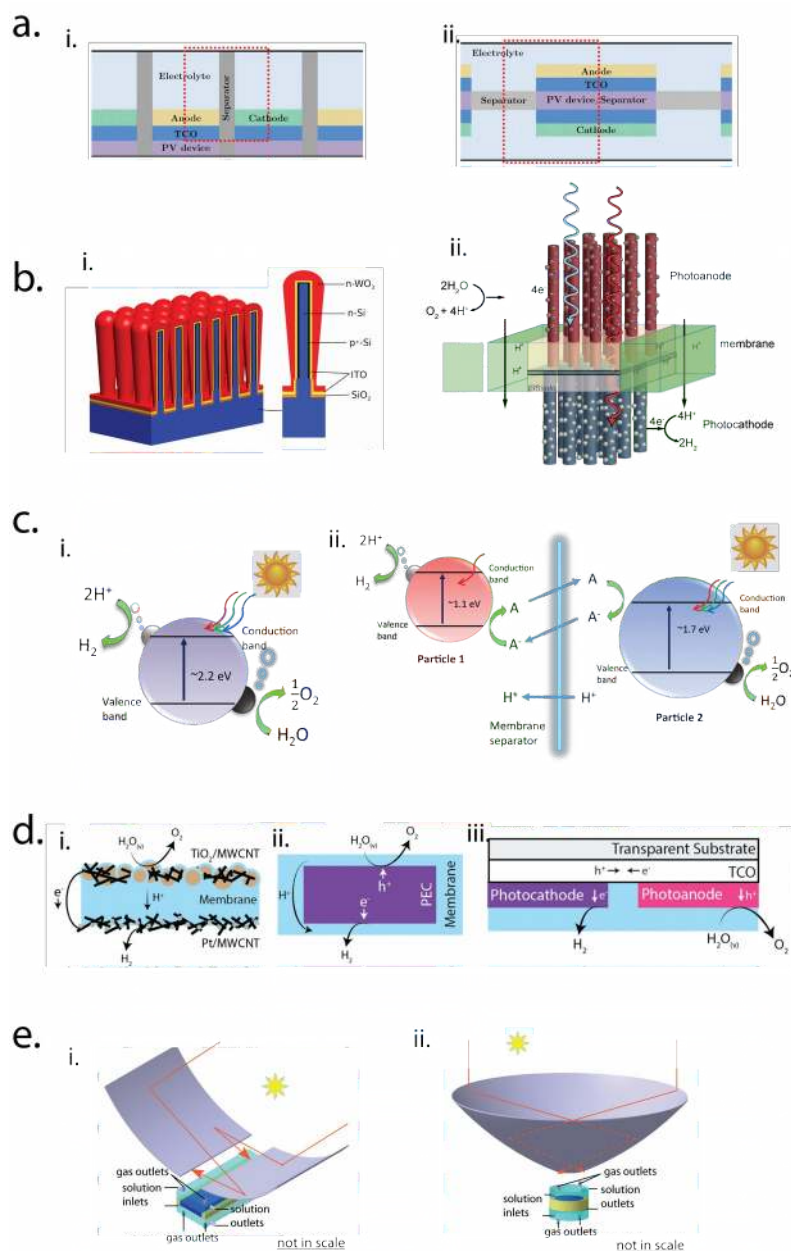
Figure 4. Schematic illustrations of various prototype architectures. (a). Macroscopic planar design (a-i). back-to-back PEC design, reproduced with permission from [13], (a-ii). side-by-side PEC design, reproduced with permission from [13]. (b). Microwire and microstructured designs.

(b-i). core-shell tandem junction microwire design, reproduced with permission from [55], (b-ii). tandem junction microwire design, reproduced with permission from [79]. (c). Particle suspension reactors. (e-i). Type 1 single vessel reactor, (e-ii). Type 2 duel vessel reactor. (d) Vapor feed design. (d-i). a photoactive MEA design, (d-ii). a membrane encapsulated PEC design, (d-iii). a side-by-side microfluidic PEC design. (e). Solar concentrator coupled PEC design. (c-i). a two-dimensional "trough" design, reproduced with permission from [10b], (c-ii). a three-dimensional "bubble wrap" design reproduced with permission from [10b].

References

[1]   aH. B. Gray, *Nat Chem* **2009**, *1*, 7-7; bN. S. Lewis, D. G. Nocera, *P Natl Acad Sci USA* **2006**, *103*, 15729-15735; cR. E. Blankenship, D. M. Tiede, J. Barber, G. W. Brudvig, G. Fleming, M. Ghirardi, M. R. Gunner, W. Junge, D. M. Kramer, A. Melis, T. A. Moore, C. C. Moser, D. G. Nocera, A. J. Nozik, D. R. Ort, W. W. Parson, R. C. Prince, R. T. Sayre, *Science* **2011**, *332*, 805-809.

[2]   aM. G. Walter, E. L. Warren, J. R. McKone, S. W. Boettcher, Q. X. Mi, E. A. Santori, N. S. Lewis, *Chem Rev* **2010**, *110*, 6446-6473; bJ. W. Ager, M. R. Shaner, K. A. Walczak, I. D. Sharp, S. Ardo, *Energ Environ Sci* **2015**, *8*, 2811-2824.

[3]   aC. R. Cox, J. Z. Lee, D. G. Nocera, T. Buonassisi, *P Natl Acad Sci USA* **2014**, *111*, 14057-14061; bJ. S. Luo, J. H. Im, M. T. Mayer, M. Schreier, M. K. Nazeeruddin, N. G. Park, S. D. Tilley, H. J. Fan, M. Gratzel, *Science* **2014**, *345*, 1593-1596.

[4]   aA. Dukic, M. Firak, *Int J Hydrogen Energ* **2011**, *36*, 7799-7806; bR. E. Clarke, S. Giddey, F. T. Ciacchi, S. P. S. Badwal, B. Paul, J. Andrews, *Int J Hydrogen Energ* **2009**, *34*, 2531-2542.

[5]   aT. Lipman, DOE, **2011**; bB. A. Pinaud, J. D. Benck, L. C. Seitz, A. J. Forman, Z. B. Chen, T. G. Deutsch, B. D. James, K. N. Baum, G. N. Baum, S. Ardo, H. L. Wang, E. Miller, T. F. Jaramillo, *Energ Environ Sci* **2013**, *6*, 1983-2002; cB. D. James, G. N. Baum, J. Perez, K. N. Baum, Directed Technologies, **2009**.

[6]   aS. Haussener, S. Hu, C. Xiang, A. Z. Weber, N. Lewis, *Energ Environ Sci* **2013**, *6*, 3605-3618; bJ. R. McKone, N. S. Lewis, H. B. Gray, *Chemistry of Materials* **2014**, *26*, 407-414.

[7]   aY. Chen, S. Hu, C. Xiang, N. S. Lewis, *Energy & Environmental Science* **2015**, *8*, 876-886; bS. Hu, C. X. Xiang, S. Haussener, A. D. Berger, N. S. Lewis, *Energ Environ Sci* **2013**, *6*, 2984-2993; cH. Doscher, J. F. Geisz, T. G. Deutsch, J. A. Turner, *Energ Environ Sci* **2014**, *7*, 2951-2956; dL. C. Seitz, Z. Chen, A. J. Forman, B. A. Pinaud, J. D. Benck, T. F. Jaramillo, *Chemsuschem* **2014**, *7*, 1372-1385; eA. Berger, R. A. Segalman, J. Newman, *Energ Environ Sci* **2014**, *7*, 1468-1476.

[8]   aJ. Jin, K. Walczak, M. R. Singh, C. Karp, N. S. Lewis, C. Xiang, *Energ Environ Sci* **2014**, *7*, 3371-3380; bM. R. Singh, K. Papadantonakis, C. X. Xiang, N. S. Lewis, *Energy & Environmental Science* **2015**, *8*, 2760-2767.

[9]   K. Walczak, Y. K. Chen, C. Karp, J. W. Beeman, M. Shaner, J. Spurgeon, I. D. Sharp, X. Amashukeli, W. West, J. Jin, N. S. Lewis, C. X. Xiang, *Chemsuschem* **2015**, *8*, 544-551.

[10]   aC. Xiang, Y. Chen, N. S. Lewis, *Energ Environ Sci* **2013**, *6*, 3713-3721; bY. K. Chen, C. X. Xiang, S. Hu, N. S. Lewis, *Journal of the Electrochemical Society, In Press* **2014**.

[11]   aK. Fujii, S. Nakamura, M. Sugiyama, K. Watanabe, B. Bagheri, Y. Nakano, *Int J Hydrogen Energ* **2013**, *38*, 14424-14432; bT. J. Jacobsson, V. Fjallstrom, M. Sahlberg, M. Edoff, T. Edvinsson, *Energy & Environmental Science* **2013**, *6*, 3676-3683; cO. Khaselev, A. Bansal, J. A. Turner, *Int J Hydrogen Energ* **2001**, *26*, 127-132; dO. Khaselev, J. A. Turner, *Science* **1998**, *280*, 425-427; eS. Licht, B. Wang, S. Mukerji, T. Soga, M. Umeno, H. Tributsch, *The Journal of Physical Chemistry B* **2000**, *104*, 8920-8924; fG. Peharz, F. Dimroth, U. Wittstadt, *Int J Hydrogen Energ* **2007**, *32*, 3248-3252; gS. W. Boettcher, E. L. Warren, M. C. Putnam, E. A. Santori, D. Turner-Evans, M. D. Kelzenberg, M. G.

43

Walter, J. R. McKone, B. S. Brunschwig, H. A. Atwater, N. S. Lewis, *J Am Chem Soc* **2011**, *133*, 1216-1219; hM. R. Shaner, S. Hu, K. Sun, N. S. Lewis, *Energ Environ Sci* **2015**, *8*, 203-207; iE. L. Warren, J. R. McKone, H. A. Atwater, H. B. Gray, N. S. Lewis, *Energ Environ Sci* **2012**, *5*, 9653-9661; jC. Liu, J. Tang, H. M. Chen, B. Liu, P. Yang, *Nano Lett* **2013**, *13*, 2989-2992; kS. A. Bonke, M. Wiechen, D. R. MacFarlane, L. Spiccia, *Energ Environ Sci* **2015**, *8*, 2791-2796.

[12]   aH. Ahmad, S. K. Kamarudin, L. J. Minggu, M. Kassim, *Renew Sust Energ Rev* **2015**, *43*, 599-610; bA. A. Ismail, D. W. Bahnemann, *Sol Energ Mat Sol C* **2014**, *128*, 85-101; cM. Ni, M. K. H. Leung, D. Y. C. Leung, K. Sumathy, *Renew Sust Energ Rev* **2007**, *11*, 401-425; dS. J. A. Moniz, S. A. Shevlin, D. J. Martin, Z. X. Guo, J. W. Tang, *Energy & Environmental Science* **2015**, *8*, 731-759; eD. M. Fabian, S. Hu, N. Singh, F. A. Houle, T. Hisatomi, K. Domen, F. E. Osterlohf, S. Ardo, *Energy & Environmental Science* **2015**, *8*, 2825-2850; fZ. S. Li, W. J. Luo, M. L. Zhang, J. Y. Feng, Z. G. Zou, *Energy & Environmental Science* **2013**, *6*, 347-370; gJ. T. Li, N. Q. Wu, *Catal Sci Technol* **2015**, *5*, 1360-1384; hX. B. Chen, S. H. Shen, L. J. Guo, S. S. Mao, *Chem Rev* **2010**, *110*, 6503-6570.

[13]   S. Haussener, C. Xiang, J. M. Spurgeon, S. Ardo, N. S. Lewis, A. Z. Weber, *Energy & Environmental Science* **2012**, *5*, 9922-9935.

[14]   J. R. Bolton, S. J. Strickler, J. S. Connolly, *Nature* **1985**, *316*, 495-500.

[15]   aJ. Newman, K. E. Thomas-Alyea, *Electrochemical Systems*, 3rd ed., John Wiley & Sons, New York, **2004**; bR. B. Bird, W. E. Stewart, E. N. Lightfoot, *Transport Phenomena*, 2nd ed., John Wiley & Sons, Inc., New York, **2002**.

[16]   S. Y. Tembhurne, M. Dumortier, S. Haussener, in *15th International Heat Transfer Conference*, Kyoto, Japan, **2014**.

[17]   H. Doscher, J. Geisz, T. Deutsch, J. A. Turner, *Energy & Environmental Science, In Press* **2014**.

[18]   H. A. Atwater, A. Polman, *Nature Materials* **2010**, *9*, 205-213.

[19]   aM. B. Cortie, A. M. McDonagh, *Chem Rev* **2011**, null-null; bC. Clavero, *Nat Photon* **2014**, *8*, 95-103.

[20]   aM. Murdoch, G. I. N. Waterhouse, M. A. Nadeem, J. B. Metson, M. A. Keane, R. F. Howe, J. Llorca, H. Idriss, *Nat Chem* **2011**, *3*, 489-492; bS. Mubeen, J. Lee, N. Singh, S. Kramer, G. D. Stucky, M. Moskovits, *Nat Nano* **2013**, *8*, 247-251.

[21]   aK. Sun, Y. Kuang, E. Verlage, B. S. Brunschwig, C. W. Tu, N. S. Lewis, *Advanced Energy Materials* **2015**; bK. Sun, M. T. McDowell, A. C. Nielander, S. Hu, M. R. Shaner, F. Yang, B. S. Brunschwig, N. S. Lewis, *The Journal of Physical Chemistry Letters* **2015**, *6*, 592-598; cK. Sun, F. H. Saadi, M. F. Lichterman, W. G. Hale, H.-P. Wang, X. Zhou, N. T. Plymale, S. T. Omelchenko, J.-H. He, K. M. Papadantonakis, B. S. Brunschwig, N. S. Lewis, *Proceedings of the National Academy of Sciences* **2015**, *112*, 3612-3617; dX. Zhou, R. Liu, K. Sun, D. Friedrich, M. T. McDowell, F. Yang, S. T. Omelchenko, F. H. Saadi, A. C. Nielander, S. Yalamanchili, K. M. Papadantonakis, B. S. Brunschwig, N. S. Lewis, *Energ Environ Sci* **2015**; eS. Hu, M. R. Shaner, J. A. Beardslee, M. Lichterman, B. S. Brunschwig, N. S. Lewis, *Science* **2014**, *344*, 1005-1009; fE. Verlage, S. Hu, R. Liu, R. J. R. Jones, K. Sun, C. Xiang, N. S. Lewis, H. A. Atwater, *Energy & Environmental Science* **2015**.

[22]   R. C. Rossi, N. S. Lewis, *The Journal of Physical Chemistry B* **2001**, *105*, 12303-12318.

[23]   aA. J. Nozik, *Annual Review of Physical Chemistry* **1978**, *29*, 189-222; bA. Heller, *Accounts Chem Res* **1981**, *14*, 154-162; cN. S. Lewis, *Annual Review of Physical Chemistry* **1991**, *42*, 543-580; dH. Gerischer, *Advances in Electrochemistry and Electrochemical Engineering, Vol. 1*, Interscience Publishers, **1961**.

[24]   Y. Surendranath, D. K. Bediako, D. G. Nocera, *Proceedings of the National Academy of Sciences* **2012**, *109*, 15617-15621.

[25]   aL. Trotochaud, T. J. Mills, S. W. Boettcher, *J Phys Chem Lett* **2013**, *4*, 931-935; bJ. M. Gregoire, C. Xiang, S. Mitrovic, X. Liu, M. Marcin, E. W. Cornell, J. Fan, J. Jin, *Journal of The Electrochemical Society* **2013**, *160*, F337-F342; cF. Svegl, B. Orel, M. G. Hutchins, K. Kalcher, *Journal of the Electrochemical Society* **1996**, *143*, 1532-1539; dB. Orel, M. Macek, F. Svegl, K. Kalcher, *Thin Solid Films* **1994**, *246*, 131-142.

[26]   A. Shinde, D. Guevarra, J. A. Haber, J. Jin, J. M. Gregoire, *Journal of Materials Research* **2014**, *FirstView*, 1-9.

[27]   A. Heller, D. E. Aspnes, J. D. Porter, T. T. Sheng, R. G. Vadimsky, *J Phys Chem-Us* **1985**, *89*, 4444-4452.

[28]   aY. K. Chen, K. Sun, H. Audesirk, C. X. Xiang, N. S. Lewis, *Energ Environ Sci* **2015**, *8*, 1736-1747; bE. Kemppainen, A. Bodin, B. Sebok, T. Pedersen, B. Seger, B. Mei, D. Bae, P. C. K. Vesborg, J. Halme, O. Hansen, P. D. Lund, I. Chorkendorff, *Energy & Environmental Science* **2015**, *8*, 2991-2999.

[29]   A. J. Bard, L. R. Faulkner, *Electrochemical Methods, Fundamentals and Applications*, 2nd edition ed., Wiley, **2000**.

[30]   C. C. L. McCrory, S. Jung, I. M. Ferrer, S. M. Chatman, J. C. Peters, T. F. Jaramillo, *J Am Chem Soc* **2015**.

[31]   aM. A. Modestino, K. A. Walczak, A. Berger, C. M. Evans, S. Haussener, C. Koval, J. S. Newman, J. W. Ager, R. A. Segalman, *Energy Environ. Sci.* **2014**, *7*, 297-301; bS. M. H. Hashemi, M. A. Modestino, D. Psaltis, *Energy & Environmental Science* **2015**, *8*, 2003-2009.

[32]   E. A. Hernandez-Pagan, N. M. Vargas-Barbosa, T. H. Wang, Y. X. Zhao, E. S. Smotkin, T. E. Mallouk, *Energy & Environmental Science* **2012**, *5*, 7582-7589.

[33]   D. A. Vermaas, M. Sassenburg, W. A. Smith, *Journal of Materials Chemistry A* **2015**, *3*, 19556-19562.

[34]   aK.-T. Jeng, Y.-C. Liu, Y.-F. Leu, Y.-Z. Zeng, J.-C. Chung, T.-Y. Wei, *Int J Hydrogen Energ* **2010**, *35*, 10890-10897; bY. Leng, G. Chen, A. J. Mendoza, T. B. Tighe, M. A. Hickner, C.-Y. Wang, *J Am Chem Soc* **2012**, *134*, 9054-9057; cM. R. Singh, J. C. Stevens, A. Z. Weber, *Journal of The Electrochemical Society* **2014**, *161*, E3283-E3296.

[35]   aK. Zeng, D. Zhang, *Progress in Energy and Combustion Science* **2010**, *36*, 307-326; bM. Carmo, D. L. Fritz, J. Mergel, D. Stolten, *Int J Hydrogen Energ* **2013**, *38*, 4901-4934; cG. Gahleitner, *Int J Hydrogen Energ* **2013**, *38*, 2039-2061; dA. Ursua, L. M. Gandia, P. Sanchis, *P Ieee* **2012**, *100*, 410-426.

[36]   M. I. Gillespie, F. van der Merwe, R. J. Kriek, *Journal of Power Sources* **2015**, *293*, 228-235.

[37]   A. Berger, J. Newman, *Journal of The Electrochemical Society* **2014**, *161*, E3328-E3340.

[38]   A. Z. Weber, *Journal of The Electrochemical Society* **2008**, *155*, B521-B531.

45

[39] K. D. Kreuer, S. J. Paddison, E. Spohr, M. Schuster, *Chemical Reviews* **2004**, *104*, 4637-4678.

[40] Y. Ma, M. Doyle, T. F. Fuller, M. M. Doeff, L. C. De Jonghe, J. Newman, *Journal of The Electrochemical Society* **1995**, *142*, 1859-1868.

[41] C. M. Evans, M. R. Singh, N. A. Lynd, R. A. Segalman, *Macromolecules* **2015**, *48*, 3303-3309.

[42] aY. Schneider, M. A. Modestino, B. L. McCulloch, M. L. Hoarfrost, R. W. Hess, R. A. Segalman, *Macromolecules* **2013**, *46*, 1543-1548; bP. Cotanda, G. Sudre, M. A. Modestino, X. C. Chen, N. P. Balsara, *Macromolecules* **2014**, *47*, 7540-7547; cA. D. Mohanty, C. Y. Ryu, Y. S. Kim, C. Bae, *Macromolecules* **2015**, *48*, 7085-7095; dK. M. Meek, S. Sharick, Y. Ye, K. I. Winey, Y. A. Elabd, *Macromolecules* **2015**, *48*, 4850-4862.

[43] aB. P. Tripathi, V. K. Shahi, *Progress in Polymer Science* **2011**, *36*, 945-979; bH. Zarrin, D. Higgins, Y. Jun, Z. Chen, M. Fowler, *The Journal of Physical Chemistry C* **2011**, *115*, 20774-20781.

[44] A. Roy, M. A. Hickner, X. Yu, Y. Li, T. E. Glass, J. E. McGrath, *Journal of Polymer Science Part B: Polymer Physics* **2006**, *44*, 2226-2239.

[45] M. B. McDonald, S. Ardo, N. S. Lewis, M. S. Freund, *Chemsuschem* **2014**, *7*, 3021-3027.

[46] K. Sun, R. Liu, E. Verlage, N. S. Lewis, C. Xiang, **2015, manuscript submitted.**

[47] aN. A. Kelly, T. L. Gibson, *Int J Hydrogen Energ* **2006**, *31*, 1658 - 1673; bH. Dotan, O. Kfir, E. Sharlin, O. Blank, M. Gross, I. Dumchin, G. Ankonina, A. Rothschild, *Nat Mater* **2013**, *12*, 158-164; cB. M. Kayes, H. A. Atwater, N. S. Lewis, *Journal of Applied Physics* **2005**, *97*, 114302.

[48] K. Sivula, *CHIMIA International Journal for Chemistry* **2013**, *67*, 155-161.

[49] J. Brillet, J.-H. Yum, M. Cornuz, T. Hisatomi, R. Solarska, J. Augustynski, M. Graetzel, K. Sivula, *Nat Photon* **2012**, *6*, 824-828.

[50] aR. E. Rocheleau, E. L. Miller, A. Misra, *Energy \& Fuels* **1998**, *12*, 3-10; bL. Tong, A. Iwase, A. Nattestad, U. Bach, M. Weidelener, G. Gotz, A. Mishra, P. Bauerle, R. Amal, G. G. Wallace, A. J. Mozer, *Energy Environ. Sci.* **2012**, *5*, 9472-9475.

[51] J. Newman, *Journal of The Electrochemical Society* **2013**, *160*, F309-F311.

[52] J. J. Turner, *Nat Mater* **2008**, *7*, 770-771.

[53] M. D. Kelzenberg, S. W. Boettcher, J. A. Petykiewicz, D. B. Turner-Evans, M. C. Putnam, E. L. Warren, J. M. Spurgeon, R. M. Briggs, N. S. Lewis, H. A. Atwater, *Nature Materials* **2010**, *9*, 239-244.

[54] C. Xiang, A. C. Meng, N. S. Lewis, *Proc Natl Acad Sci U S A* **2012**, *109*, 15622-15627.

[55] M. R. Shaner, K. T. Fountaine, S. Ardo, R. H. Coridan, H. A. Atwater, N. S. Lewis, *Energ Environ Sci* **2014**, *7*, 779-790.

[56] aM. C. Putnam, S. W. Boettcher, M. D. Kelzenberg, D. B. Turner-Evans, J. M. Spurgeon, E. L. Warren, R. M. Briggs, N. S. Lewis, H. A. Atwater, *Energy & Environmental Science* **2010**, *3*, 1037; bJ. Wallentin, N. Anttu, D. Asoli, M. Huffman, I. Aberg, M. H. Magnusson, G. Siefer, P. Fuss-Kailuweit, F. Dimroth, B. Witzigmann, H. Q. Xu, L. Samuelson, K. Deppert, M. T. Borgstrom, *Science* **2013**, *339*, 1057-1060; cM. Yao, N. Huang, S. Cong, C. Y. Chi, M. A. Seyedi, Y. T. Lin, Y. Cao, M. L. Povinelli, P. D. Dapkus, C. Zhou, *Nano Lett* **2014**, *14*, 3293-3303; dZ. Fan, H. Razavi, J. W. Do, A.

Moriwaki, O. Ergen, Y. L. Chueh, P. W. Leu, J. C. Ho, T. Takahashi, L. A. Reichertz, S. Neale, K. Yu, M. Wu, J. W. Ager, A. Javey, *Nat Mater* **2009**, *8*, 648-653.

[57] aN. C. Strandwitz, D. B. Turner-Evans, A. C. Tamboli, C. T. Chen, H. A. Atwater, N. S. Lewis, *Advanced Energy Materials* **2012**, *2*, 1109-1116; bC. T. Chen, D. B. Turner-Evans, H. Emmer, S. Aloni, H. A. Atwater, *Ieee Phot Spec Conf* **2013**, 3397-3401; cA. C. Tamboli, M. Malhotra, G. M. Kimball, D. B. Turner-Evans, H. A. Atwater, *Applied Physics Letters* **2010**, *97*, 221914.

[58] X. Wang, K.-Q. Peng, Y. Hu, F.-Q. Zhang, B. Hu, L. Li, M. Wang, X.-M. Meng, S.-T. Lee, *Nano Lett* **2014**, *14*, 18-23.

[59] D. M. Fabian, S. Hu, N. Singh, F. A. Houle, T. Hisatomi, K. Domen, F. E. Osterloh, S. Ardo, *Energy Environ. Sci.* **2015**, *8*, 2825-2850.

[60] Z. G. Zou, J. H. Ye, K. Sayama, H. Arakawa, *Nature* **2001**, *414*, 625-627.

[61] X. C. Wang, K. Maeda, Y. Lee, K. Domen, *Chem Phys Lett* **2008**, *457*, 134-136.

[62] K. Maeda, K. Teramura, K. Domen, *J Catal* **2008**, *254*, 198-204.

[63] L. B. Liao, Q. H. Zhang, Z. H. Su, Z. Z. Zhao, Y. N. Wang, Y. Li, X. X. Lu, D. G. Wei, G. Y. Feng, Q. K. Yu, X. J. Cai, J. M. Zhao, Z. F. Ren, H. Fang, F. Robles-Hernandez, S. Baldelli, J. M. Bao, *Nat Nanotechnol* **2014**, *9*, 69-73.

[64] J. Liu, Y. Liu, N. Y. Liu, Y. Z. Han, X. Zhang, H. Huang, Y. Lifshitz, S. T. Lee, J. Zhong, Z. H. Kang, *Science* **2015**, *347*, 970-974.

[65] Y. Sasaki, H. Nemoto, K. Saito, A. Kudo, *J Phys Chem C* **2009**, *113*, 17536-17542.

[66] T. F. Yeh, C. Y. Teng, S. J. Chen, H. S. Teng, *Adv Mater* **2014**, *26*, 3297-+.

[67] K. Maeda, M. Higashi, D. L. Lu, R. Abe, K. Domen, *J Am Chem Soc* **2010**, *132*, 5858-5868.

[68] W. Y. Wang, J. Chen, C. Li, W. M. Tian, *Nat Commun* **2014**, *5*.

[69] Y. Sasaki, H. Kato, A. Kudo, *J Am Chem Soc* **2013**, *135*, 5441-5449.

[70] K. Maeda, K. Domen, *J Phys Chem Lett* **2010**, *1*, 2655-2661.

[71] A. Agiral, H. S. Soo, H. Frei, *Chemistry of Materials* **2013**, *25*, 2264-2273.

[72] aM. A. Modestino, S. Haussener, *Annual Review of Chemical and Biomolecular Engineering* **2015**, *6*, 13-34; bJ. Rongé, T. Bosserez, L. Huguenin, M. Dumortier, S. Haussener, J. A. Martens, *Oil & Gas Science and Technology–Revue d'IFP Energies nouvelles* **2015**.

[73] J. M. Spurgeon, N. S. Lewis, *Energy & Environmental Science* **2011**, *4*, 2993-2998.

[74] aJ. M. Spurgeon, M. G. Walter, J. Zhou, P. A. Kohl, N. S. Lewis, *Energy & Environmental Science* **2011**, *4*, 1772-1780; bM. R. Shaner, J. R. McKone, H. B. Gray, N. S. Lewis, *Energy & Environmental Science* **2015**.

[75] aM. A. Modestino, D. K. Paul, S. Dishari, S. A. Petrina, F. I. Allen, M. A. Hickner, K. Karan, R. A. Segalman, A. Z. Weber, *Macromolecules* **2013**, *46*, 867-873; bM. A. Modestino, A. Kusoglu, A. Hexemer, A. Z. Weber, R. A. Segalman, *Macromolecules* **2012**, *45*, 4681-4688; cS. A. Eastman, S. Kim, K. A. Page, B. W. Rowe, S. Kang, C. L. Soles, K. G. Yager, *Macromolecules* **2012**, *45*, 7920-7930; dM. Bass, A. Berman, A. Singh, O. Konovalov, V. Freger, *Macromolecules* **2011**, *44*, 2893-2899; eD. K. Paul, A. Fraser, K. Karan, *Electrochemistry Communications* **2011**, *13*, 774-777; fA. Kusoglu, D. Kushner, D. K. Paul, K. Karan, M. A. Hickner, A. Z. Weber, *Advanced Functional*

47

Materials **2014**, *24*, 4763-4774; gF. I. Allen, L. R. Comoli, A. Kusoglu, M. A. Modestino, A. M. Minor, A. Z. Weber, *ACS Macro Letters* **2015**, *4*, 1-5.

[76]   M. A. Modestino, M. Dumortier, M. Hashemi, S. Haussener, C. Moser, D. Psaltis, *Lab on a Chip* **2015**, *15*, 2287-2296.

[77]   S. M. Sze, *Physics of Semiconductor Devices*, Third Edition ed., John Wiley and Sons, New York, **1981**.

[78]   V. M. Aroutiounian, V. M. Arakelyan, G. E. Shahnazaryan, *Sol Energy* **2005**, *78*, 581-592.

[79]   E. L. Warren, H. A. Atwater, N. S. Lewis, *J Phys Chem C* **2014**, *118*, 747-759.

48
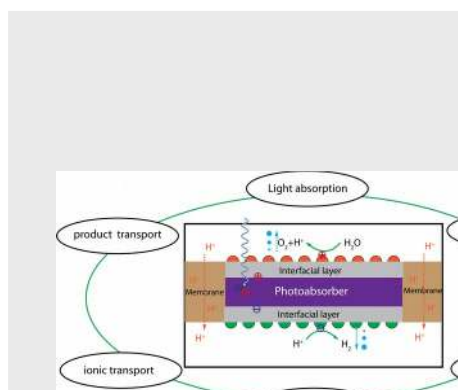
Chengxiang Xiang,* Adam Z. Weber*
Shane Ardo, Alan Berger, YiKai Chen,
Robert Coridan, Katherine T. Fountaine,
Sophia Haussener, Shu Hu, Rui Liu,
Nathan S. Lewis, Miguel A. Modestino,
Matthew M. Shaner, Meenesh R. Singh,
John C. Stevens, Ke Sun, Karl Walczak

Page No. – Page No.

Modeling, Simulation, and Implementation of Solar-Driven Water-Splitting Devices